Theoretical and Applied Mechanics Letters 6 (2016) 6–10

Contents lists available at ScienceDirect

Theoretical and Applied Mechanics Letters

journal homepage: www.elsevier.com/locate/taml

Letter

Adhesion-governed buckling of thin-film electronics on soft tissues

Bo Wang, Shuodao Wang *

School of Mechanical and Aerospace Engineering, Oklahoma State University, Stillwater, OK, 74078, USA

HIGHLIGHTS

- Adhesion-governed buckling physics for thin-film on elastomer.
- The transitions between buckling modes are predicted analytically.
- Mechanics discussed in the context of bio-integrated electronics applications.

ARTICLE INFO

Article history:
Received 13 October 2015
Received in revised form
14 November 2015
Accepted 20 November 2015
Available online 24 December 2015

Keywords:
Stretchable electronics
Bio-electronics
Buckling
Work of adhesion
Bio-interface

ABSTRACT

Stretchable/flexible electronics has attracted great interest and attention due to its potentially broad applications in bio-compatible systems. One class of these ultra-thin electronic systems has found promising and important utilities in bio-integrated monitoring and therapeutic devices. These devices can conform to the surfaces of soft bio-tissues such as the epidermis, the epicardium, and the brain to provide portable healthcare functionalities. Upon contractions of the soft tissues, the electronics undergoes compression and buckles into various modes, depending on the stiffness of the tissue and the strength of the interfacial adhesion. These buckling modes result in different kinds of interfacial delamination and shapes of the deformed electronics, which are very important to the proper functioning of the bio-electronic devices. In this paper, detailed buckling mechanics of these thin-film electronics on elastomeric substrates is studied. The analytical results, validated by experiments, provide a very convenient tool for predicting peak strain in the electronics and the intactness of the interface under various conditions.

Stretchable electronics, being as stretchable and flexible as soft tissues, has enabled many important applications, such as [1–8] eyeball-like digital cameras [9,10], sensitive robotic skins [11,12], smart surgical gloves [13], comfortable skin sensor [14], and structural health monitoring devices [15]. Among these applications, some of the most important ones are the bio-integrated monitoring and therapeutic devices that can conform to the surfaces of soft bio-tissues such as the epidermis [16], the epicardium [17], and the brain [18], which provide promising options for long-term and portable healthcare devices. Upon contractions of the soft tissues, the electronics undergoes compression and buckles into various modes [19,20]. A few important mechanics models were developed to study the buckling problems on similar film-on-elastomer systems. Jiang et al. [2] studied the buckling behavior of strongly-bonded film-on-elastomer structures and predicted the maximum strain in the thin film to prevent fracture. Wang et al. [1] described local and global buckling modes for one-dimensional thin films or two-dimensional thin membranes on elastomers, and obtained the analytical critical conditions for separating the two buckling modes. Cheng et al. [21] introduced a bi-layer elastomeric substrate (a soft layer laminated on top of a relatively stiff one) that yields high levels of stretchability, and discussed the buckling and post-buckling behaviors. To achieve optimum bio-compatibility, Ko et al. [22] and Wang et al. [23] introduced advanced strategies to wrap thin-film electronics onto arbitrarily curvilinear shapes, for which Wang et al. [23] developed an analytical model to study the buckling patterns, and showed that the buckling behaviors are governed by the strength of the interface and the level of the compressive strain.

These important mechanics models indicate that the buckling behavior of these film-on-elastomer structures is related to the applied strain, the material and geometric parameters of the film, the stiffness of the elastomer, as well as the strength of the interfacial adhesion. In the context of bio-electronics applications where the tissues are the elastomeric substrate, *the stiffness of the tissues* and *the strength of the interface* can vary in a very wide range due to the type of tissues and changes in temperature, moisture, and bio-chemical activities. *The intactness of the interface* is of great importance to the functioning of electronic devices

* Corresponding author.
E-mail address: shuodao.wang@okstate.edu (S. Wang).

http://dx.doi.org/10.1016/j.taml.2015.11.010

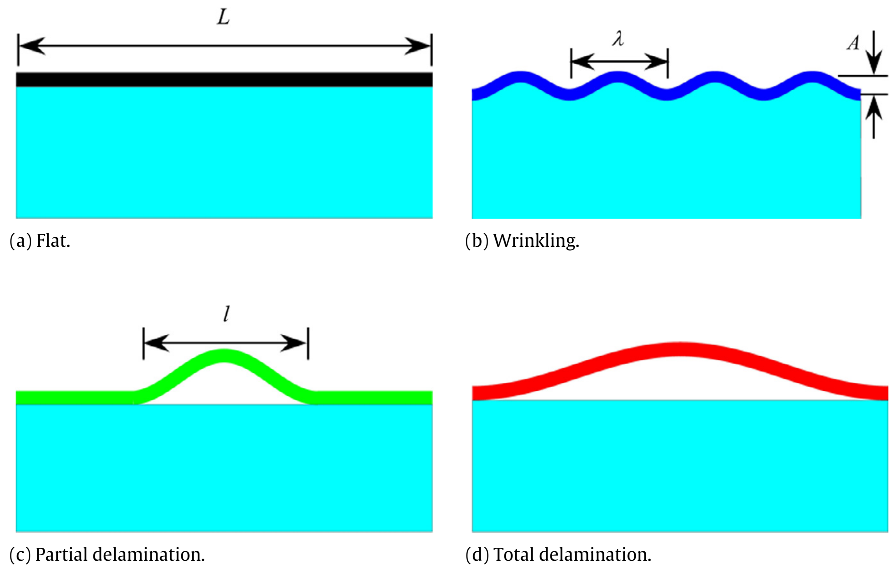

Fig. 1. The four buckling modes: (a) *flat*; (b) *wrinkling*; (c) *partial delamination*; (d) *total delamination*.

that rely on intimate contact and coupling to the tissues. Detailed mechanics analysis of the buckling physics that accounts for any tissue stiffness and any interfacial adhesion is presented in this study to predict the intactness of the bio-electronics interfaces.

The various buckling modes in the previous work [1,2,16–20] can be categorized into the four modes shown in Fig. 1. Under none to minor compression, the film does not buckle and remains *flat* (Fig. 1(a)); as the compression increases, the film wrinkles into multiple small waves on top of the elastomer but does not delaminate from the interface, which we refer to as the *wrinkling* mode (Fig. 1(b)); under further compression, the multiple waves merge into one and cause the film to partially delaminate from the interface, which is the *partial delamination* mode (Fig. 1(c)); more compression eventually causes the film to delaminate totally from the interface, which we define as the *total delamination* mode in this study (Fig. 1(d)). The energies of these different buckling modes are formulated and then compared in the next section to explain transitions between them.

Here we consider a film-structure of length L, thickness h, and Young's modulus E laminated on top of a soft substrate of Young's modulus E_s, and the work of adhesion for the interface is γ, and the structure is under a compressive applied strain of $|\varepsilon|$. By assuming a sinusoidal buckling shape of wavelength $0 < l < L$ (Fig. 1(c)), Wang et al. [23] analyzed the energies for the *flat, partial* and *total delamination* modes. Their analysis is elaborated in the Supplementary Information and summarized in the following. All the energies are normalized by $ELh\varepsilon_c^2$ for convenience, where $\varepsilon_c = \left(\pi^2 h^2\right) / \left(3L^2\right)$. We also define the following non-dimensional quantities: the normalized applied strain $e = |\varepsilon| / \varepsilon_c$, the normalized critical wrinkling strain $e_w = (3E_s/E)^{2/3} / (4\varepsilon_c)$, the normalized adhesion $g = \gamma / \left(8Eh\varepsilon_c^2\right)$ and the normalized delaminated length $a = l/L$.

For the *flat* mode, the total energy of the system consists of the membrane energy of the film, and the adhesion energy of the entire interface, and is obtained as

$$U^{\text{flat}} = \frac{1}{2}e^2 - 8g. \tag{1}$$

For the *partial delamination* mode, the total energy consists of the membrane and bending energy of the film and the adhesion energy of the un-delaminated part of the interface [length of $(L-l)$], and is obtained as

$$U^{\text{part.delam}} = ea^{-2} - \frac{1}{2}a^{-4} - 8g\,(1-a)\,. \tag{2}$$

Energy minimization with respect to a requires the first derivative of Eq. (2) to be zero and the second derivative to be greater than zero, therefore a can be solved from

$$\begin{cases} 4ga^5 - ea^2 + 1 = 0, \\ \sqrt{3/\,(5e)} < a \le 1, \end{cases} \tag{3}$$

where $a \le 1$ is due to the constraint that $l \le L$.

For the *total delamination* mode, the energy consists of the membrane and bending energy of the film, and is obtained as

$$U^{\text{tot.delam}} = e - \frac{1}{2}. \tag{4}$$

In this study, we find that a fourth buckling mode, i.e. the *wrinkling* mode, exists under certain conditions. Following similar approach of Jiang et al. [2], the energy of this mode consists of the membrane and bending energies of the film, the strain energy of the substrate, as well as the adhesion energy of the interface, and can be obtained analytically as

$$U^{\text{wrinkle}} = e_w\left(e - \frac{1}{2}e_w\right) - 8g. \tag{5}$$

It should be noted that this energy only exists when the applied strain exceeds the critical buckling strain, namely $e > e_w$.

Here we adopt a typical case of $e_w = 4$ and $g = 3$ to facilitate the discussion. Figure 2 shows the four energy curves versus the normalized strain e. All the curves are obtained analytically from Eqs. (1) to (5), except for the case of local buckling (blue curve). It is clearly shown in Fig. 2 that for very small strain e, the flat mode has the lowest energy. As e increases, *wrinkling, partial delamination* and then *total delamination* modes become the lowest energy state in sequence. Intersections of the above energy curves are important because they indicate the transitions from one buckling mode to another. Depending on the values of e_w and g, there are 6 possible intersections between these curves, which are found below.

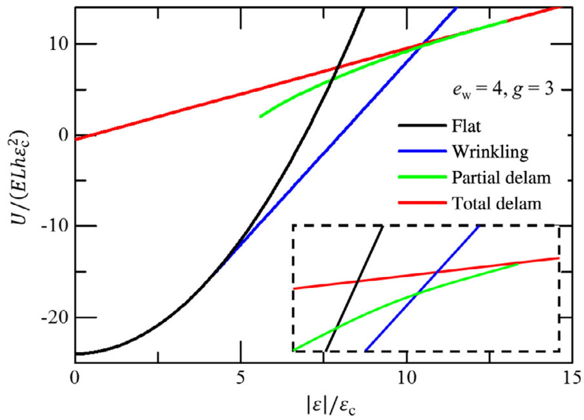

Fig. 2. Normalized energy curves of the four buckling modes versus normalized applied strain. The inset in the dashed box shows illustrative details of the intersection points (not to scale) between the four curves. (For interpretation of the references to color in this figure legend, the reader is referred to the web version of this article.)

The intersection between *flat* and *wrinkling* (black and green curves) is found by setting $U^{\text{flat}} = U^{\text{wrinkle}}$ (Eqs. (1) and (5)), which yields

$$e_{\text{flat-wrinkle}} = e_{\text{w}}. \tag{6}$$

The intersection between *flat* and *total delamination* (black and red curves) is found by setting $U^{\text{flat}} = U^{\text{tot.delam}}$ (Eqs. (1) and (4)), which yields

$$e_{\text{flat-tot.delam}} = 4\sqrt{g} + 1. \tag{7}$$

The intersection between *wrinkling* and *total delamination* (black and red curves) is found by setting $U^{\text{wrinkle}} = U^{\text{tot.delam}}$ (Eqs. (4) and (5)), which yields

$$e_{\text{wrinkle-tot.delam}} = \frac{16g - 1 + e_{\text{w}}^2}{2e_{\text{w}} - 2}. \tag{8}$$

Following the analysis of Wang et al. [23], the intersection between *flat* and *partial delamination* is found to be

$$e_{\text{flat-part.delam}} = 5g^{2/5}, \tag{9}$$

and that between *partial delamination* and *total delamination* is

$$e_{\text{part-tot.delm}} = 4g + 1. \tag{10}$$

The intersection between *wrinkling* and *partial delamination* cannot be obtained analytically because the energy of partial delamination needs to be solved numerically from Eqs. (2) and (3). Here an approximate solution is obtained. We notice that the blue curve for partial delamination is very close to a linear line, and two points on this line can be given analytically by Eqs. (9) and (10) and Eqs. (1) and (4) as

$$\begin{cases} \left(5g^{2/5},\ \dfrac{25}{2}g^{4/5} - 8g\right) \\ \quad \text{intersection of green and black curves,} \\ \left(4g + 1,\ 4g + \dfrac{1}{2}\right) \\ \quad \text{intersection of green and red curves.} \end{cases} \tag{11}$$

The energy curve for *partial delamination* can be approximated by the straight line connecting the two points in Eq. (11). The intersection point between this line and the wrinkling curve can be then obtained analytically as

$$e_{\text{wrinkle-part.delam}} = \frac{f \cdot 5g^{2/5} - e_{\text{w}}^2 - 25g^{4/5}}{f - 2e_{\text{w}}}, \tag{12}$$

where $f = \left(24g + 1 - 25g^{4/5}\right) / \left(4g + 1 - 5g^{2/5}\right)$. It is verified in the next sub-section that Eq. (12) agrees very well with numerical solution obtained by Eqs. (2), (3) and (5).

By carefully comparing the energies, one can determine which buckling mode has the lowest energy. However, the relations between these energies depend on the values of e_{w} and g, and therefore require careful investigation of various cases. We categorize these cases by the value of $e_{\text{w}} = (3E_s/E)^{2/3} / (4\varepsilon_c)$ (an indication of relative stiffness of the substrate) as the following.

(1) $0 < e_{\text{w}} \le 1$: for extremely soft substrate, it is found that the energy of the *wrinkling* mode is always lower than those of *partial* and *total delamination* modes. Therefore, the deformation map is obtained from Eq. (6) as

$$\text{for } 0 < e_{\text{w}} \le 1, \quad \begin{cases} \textit{flat}, & \text{when } e < e_{\text{w}} \\ \textit{wrinkling}, & \text{when } e \ge e_{\text{w}}. \end{cases} \tag{13}$$

(2) $1 < e_{\text{w}} \le 3$: for soft substrate, it is found that the *wrinkling* mode only exists for relatively strong adhesion of $g > (e_{\text{w}} - 1)^2 / 16$ and *partial delamination* does not happen. For weak adhesion of $g \le (e_{\text{w}} - 1)^2 / 16$, transition strain for *flat*-(*total delamination*) can be found by Eq. (7); for stronger adhesion, transition strain for *flat*–*wrinkling* and *wrinkling*–(*total delamination*) are given by Eqs. (6) and (8):

for $1 < e_{\text{w}} \le 3$,

$$\begin{cases} g \le (e_{\text{w}} - 1)^2/16, \\ \quad \begin{cases} \textit{flat}, & \text{when } e < 4\sqrt{g} + 1, \\ \textit{total delamination}, & \text{when } e \ge 4\sqrt{g} + 1, \end{cases} \\ g > (e_{\text{w}} - 1)^2/16, \\ \quad \begin{cases} \textit{flat}, & \text{when } e < e_{\text{w}} \\ \textit{wrinkling}, & \text{when } e_{\text{w}} \le e < \dfrac{16g - 1 + e_{\text{w}}^2}{2e_{\text{w}} - 2}, \\ \textit{total delamination}, & \text{when } e \ge \dfrac{16g - 1 + e_{\text{w}}^2}{2e_{\text{w}} - 2}. \end{cases} \end{cases} \tag{14}$$

(3) $3 < e_{\text{w}} \le 5$: the conclusions are the same as Case 2 for weak adhesion of $g \le (e_{\text{w}} - 1)^2 / [8(e_{\text{w}} - 3)]$. For stronger adhesion, the transitions from *flat* to *wrinkling*, then to *partial* and *total delamination* modes can be obtained from Eqs. (6), (10) and (12) as

for $3 < e_{\text{w}} \le 5$,

$$\begin{cases} g \le \dfrac{(e_{\text{w}} - 1)^2}{8(e_{\text{w}} - 3)}, & \text{same as Case 2,} \\ g > \dfrac{(e_{\text{w}} - 1)^2}{8(e_{\text{w}} - 3)}, \\ \quad \begin{cases} \textit{flat}, & \text{when } e < e_{\text{w}}, \\ \textit{wrinkling}, & \text{when } e_{\text{w}} \le e < e_{\text{wrinkle-part.delam}}, \\ \textit{partial delam}, & \text{when } e_{\text{wrinkle-part.delam}} \le e < 4g + 1, \\ \textit{total delam}, & \text{when } e \ge 4g + 1. \end{cases} \end{cases} \tag{15}$$

(4) $e_{\text{w}} > 5$: for relatively stiffer substrate (note: its Young's modulus is still four to five orders of magnitude lower than that of the film), the conclusions are the same as the results of Wang et al. [23] for weak adhesion of $g \le (e_{\text{w}}/5)^{5/2}$. For adhesion stronger than that, the transitions are the same as in Case 3:

$$\text{for } e_{\text{w}} > 5, \quad \begin{cases} g \le (e_{\text{w}}/5)^{5/2}, & \text{same as Ref. [22],} \\ g > (e_{\text{w}}/5)^{5/2}, & \text{same as Case 3.} \end{cases} \tag{16}$$

In summary, based on the relative stiffness of the elastomer [indicated by the value of $e_{\text{w}} = (3E_s/E)^{2/3} / (4\varepsilon_c)$], the normalized adhesion $g = \gamma / \left(8Eh\varepsilon_c^2\right)$, and the normalized strain $e = |\varepsilon| / \varepsilon_c$, the buckling modes can be determined from Eqs. (13) to (16). These equations are plotted as the deformation maps [e versus g, namely $|\varepsilon| / \varepsilon_c$ versus $\gamma / \left(8Eh\varepsilon_c^2\right)$] in Fig. 3. It should be noted that the range of e_{w} determines the pattern of the map, and in

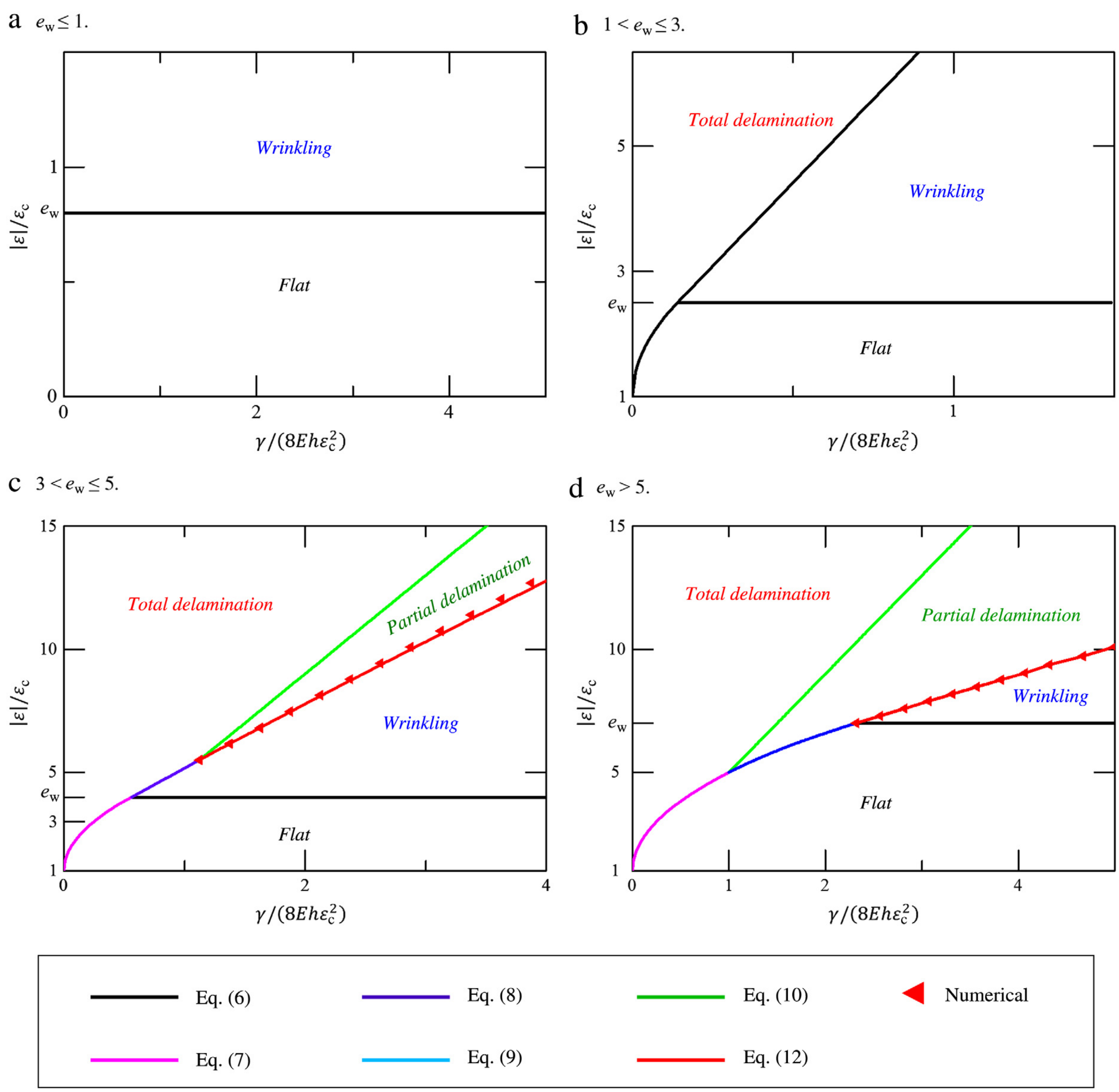

Fig. 3. Deformation maps ($|\varepsilon|/\varepsilon_c$ versus $\gamma/\left(8Eh\varepsilon_c^2\right)$) that separate the four buckling modes for various values of e_w; the plots are generated for representative e_w values of (a) 0.8; (b) 2.5; (c) 4.0; (d) 7.0. (For interpretation of the references to color in this figure legend, the reader is referred to the web version of this article.)

each map the value of e_w determines location of the black line. Figure 3 shows clearly the transitions of the four buckling modes under various conditions. It should be noted that the approximate analytical solution given by Eq. (12) (solid red line in Fig. 3(c), (d)) agrees very well with the results obtained numerically (red triangle dots) from Eqs. (2), (3) and (5).

Here we use the example in the previous studies [21,22] to show the utility of the presented results. The material and geometric and mechanical properties [22,23] are $E = 2.5$ GPa, $h = 1.4\ \mu$m, $L = 150\ \mu$m, $E_s = 2.0$ MPa, and $\gamma = 0.16$ J/m^2, which correspond to the normalized values of $e_w = 15.6$ and $g = 69.6$. Under these two conditions, Eq. (16) applies and gives the following results (these can also be obtained from Fig. 3(d)):

$$\begin{cases} \textit{flat}, & \text{when } |\varepsilon| < 0.45\%, \\ \textit{wrinkling}, & \text{when } 0.45\% \leq |\varepsilon| < 0.92\%, \\ \textit{partial delam}, & \text{when } 0.92\% \leq |\varepsilon| < 8.0\%, \\ \textit{total delam}, & \text{when } |\varepsilon| \geq 8.0\%. \end{cases}$$

These results agree very well with experimental observance shown in Fig. 4: the film is *flat* (Fig. 4(a)) before compression is applied; under very small strain it *wrinkles* into multiple waves (Fig. 4(b)) and then quickly transits to the *partial delamination* mode (Fig. 4(c)); when $|\varepsilon|$ exceeds about 8.5% [23], the film *totally delaminated* from the substrate (Fig. 4(d)), which agrees very well with the 8.0% strain predicted by the analytical model. It should be noted that there may exist another buckling mode between the *wrinkling* and *partial delamination* modes, in which the film delaminates from the substrate from multiple locations. However, since the transitions happen at very similar strain levels, we propose to adopt the simplified model presented here.

The deformed shape of the film and the peak strain for the *flat*, *partial/total delamination* modes are analyzed in detail by Wang et al. [23]. For the *wrinkling* mode, Jiang's analysis [2] shows that the wrinkling wavelength λ and amplitude A can be obtained by

$$\begin{cases} \lambda = 2\pi h\left(\dfrac{E}{3E_s}\right)^{1/3}, \\ A = h\sqrt{4|\varepsilon|\left(\dfrac{E}{3E_s}\right)^{2/3} - 1}, \end{cases} \tag{17}$$

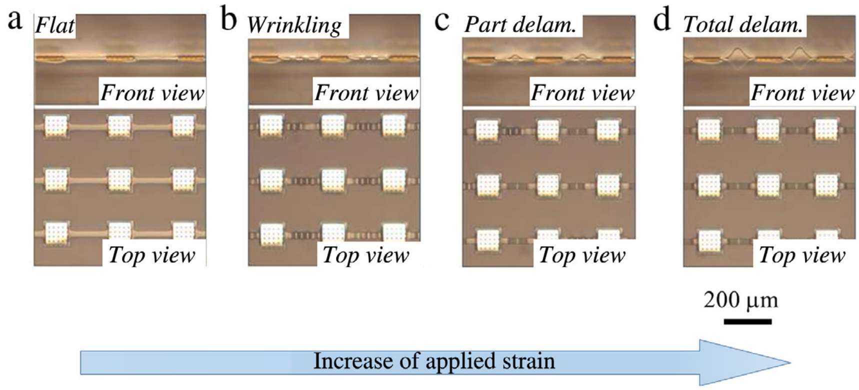

Fig. 4. Experimental images of the four buckling modes.

which gives the wavelength to be 67.5 μm and agrees reasonably with 56.8 μm from experiments (Fig. 4(b)). This predicts 2–3 waves over the total span of $L = 150$ μm, which again agrees with experimental observations (only the middle wave of the three waves in Fig. 4(b) spans for an entire wavelength of λ). Therefore, for the *wrinkling* mode, we propose to follow Jiang's approach in Ref. [2] to analyze the maximum strain to prevent fracture of the film structure.

The deformation maps shown in Fig. 3 are very important for the design of bio-integrated electronics, in the sense that they predict the buckling modes for any materials under any adhesion conditions. One crucial information they predict is the onset of interfacial delamination, indicated in these figures by the lower bounds of *partial* and *total delamination* modes (magenta, purple, cyan and red curves).

In this paper, an analytical model is established for thin-film on elastomer structures in the context of bio-integrated electronics applications. Under different conditions in interfacial adhesion, stiffness of the elastomer (tissues) and the levels of compressive strain, the thin film buckles into various modes. The transitions between these modes are predicted analytically, and summarized in four deformation maps. The lower bounds of the *partial* and *total delamination* modes predict the onset of interfacial delamination, which sets design criteria to avoid delamination and achieve intimate and conformal contact to bio-tissues. The analytically predicted information on deformation modes, maximum strain, and interfacial intactness, are important to the design and optimization of high performance bio-integrated electronics.

Acknowledgment

The authors acknowledge partial support of this research by the National Natural Science Foundation of China (Grants 11272260, 11172022, 11572022, 51075327, 11302038).

Appendix A. Supplementary data

Supplementary material related to this article can be found online at http://dx.doi.org/10.1016/j.taml.2015.11.010.

References

[1] S. Wang, J. Song, D.-H. Kim, et al., Local versus global buckling of thin films on elastomeric substrates, Appl. Phys. Lett. 93 (2008) 023126. http://dx.doi.org/10.1063/1.2956402.

[2] H. Jiang, D.-Y. Khang, J. Song, et al., Finite deformation mechanics in buckled thin films on compliant supports, Proc. Natl. Acad. Sci. 104 (2007) 15607–15612. http://dx.doi.org/10.1073/pnas.0702927104.

[3] J. Xiao, A. Carlson, Z.J. Liu, et al., Analytical and experimental studies of the mechanics of deformation in a solid with a wavy surface profile, J. Appl. Mech. 77 (2009) 011003–011003-6, http://dx.doi.org/10.1115/1.3132184.

[4] Y. Zhang, S. Xu, H. Fu, et al., Buckling in serpentine microstructures and applications in elastomer-supported ultra-stretchable electronics with high areal coverage, Soft Matter 9 (2013) 8062–8070. http://dx.doi.org/10.1039/C3SM51360B.

[5] Z. Li, Y. Wang, J. Xiao, Mechanics of curvilinear electronics and optoelectronics, Curr. Opin. Solid State Mater. Sci. 3 (2015) 171–189. http://dx.doi.org/10.1016/j.cossms.2015.01.003.

[6] S. Xu, Z. Yan, K.-I. Jang, et al., Assembly of micro/nanomaterials into complex, three-dimensional architectures by compressive buckling, Science 347 (2015) 154–159. http://dx.doi.org/10.1126/science.1260960.

[7] Y. Xue, Y. Zhang, X. Feng, et al., A theoretical model of reversible adhesion in shape memory surface relief structures and its application in transfer printing, J. Mech. Phys. Solids 77 (2015) 27–42. http://dx.doi.org/10.1016/j.jmps.2015.01.001.

[8] Z. Li, J. Xiao, Mechanics and optics of stretchable elastomeric microlens array for artificial compound eye camera, J. Appl. Phys. 117 (2015) 014904. http://dx.doi.org/10.1063/1.4905299.

[9] H.C. Ko, M.P. Stoykovich, J. Song, et al., A hemispherical electronic eye camera based on compressible silicon optoelectronics, Nature 454 (2008) 748–753. http://dx.doi.org/10.1038/nature07113.

[10] G. Shin, I. Jung, V. Malyarchuk, et al., Micromechanics and advanced designs for curved photodetector arrays in hemispherical electronic-eye cameras, Small 6 (2010) 851–856. http://dx.doi.org/10.1002/smll.200901350.

[11] S. Wagner, S.P. Lacour, J. Jones, et al., Electronic skin: architecture and components, Physica E 25 (2004) 326–334. http://dx.doi.org/10.1016/j.physe.2004.06.032.

[12] S.P. Lacour, J. Jones, Z. Suo, et al., Design and performance of thin metal film interconnects for skin-like electronic circuits, IEEE Electron Device Lett. 25 (2004) 179–181. http://dx.doi.org/10.1109/LED.2004.825190.

[13] T. Someya, T. Sekitani, S. Iba, et al., A large-area, flexible pressure sensor matrix with organic field-effect transistors for artificial skin applications, Proc. Natl. Acad. Sci. USA 101 (2004) 9966–9970. http://dx.doi.org/10.1073/pnas.0401918101.

[14] S. Xu, Y. Zhang, L. Jia, et al., Soft microfluidic assemblies of sensors, circuits, and radios for the skin, Science 344 (2014) 70–74. http://dx.doi.org/10.1126/science.1250169.

[15] A. Nathan, B. Park, A. Sazonov, et al., Amorphous silicon detector and thin film transistor technology for large-area imaging of X-rays, Microelectron. J. 31 (2000) 883–891. http://dx.doi.org/10.1016/S0026-2692(00)00082-3.

[16] D.-H. Kim, N. Lu, R. Ma, et al., Epidermal electronics, Science 333 (2011) 838–843. http://dx.doi.org/10.1126/science.1206157.

[17] L. Xu, S.R. Gutbrod, A.P. Bonifas, et al., 3D multifunctional integumentary membranes for spatiotemporal cardiac measurements and stimulation across the entire epicardium, Nature Commun. 5 (2014) 3329. http://dx.doi.org/10.1038/ncomms4329.

[18] J. Viventi, D.-H. Kim, L. Vigeland, et al., Flexible, foldable, actively multiplexed, high-density electrode array for mapping brain activity in vivo, Nat. Neurosci. 14 (2011) 1599–1605. http://dx.doi.org/10.1038/nn.2973.

[19] Z.Y. Huang, W. Hong, Z. Suo, Nonlinear analyses of wrinkles in a film bonded to a compliant substrate, J. Mech. Phys. Solids 53 (2005) 2101–2118. http://dx.doi.org/10.1016/j.jmps.2005.03.007.

[20] S. Wang, M. Li, J. Wu, et al., Mechanics of epidermal electronics, J. Appl. Mech. 79 (2012) 031022–031022-6, http://dx.doi.org/10.1115/1.4005963.

[21] H. Cheng, Y. Zhang, K.-C. Hwang, et al., Buckling of a stiff thin film on a pre-strained bi-layer substrate, Int. J. Solids Struct. 51 (2014) 3113–3118. http://dx.doi.org/10.1016/j.ijsolstr.2014.05.012.

[22] H.C. Ko, G. Shin, S. Wang, et al., Curvilinear electronics formed using silicon membrane circuits and elastomeric transfer elements, Small 5 (2009) 2703–2709. http://dx.doi.org/10.1002/smll.200900934.

[23] S. Wang, J. Xiao, J. Song, et al., Mechanics of curvilinear electronics, Soft Matter 6 (2010) 5757–5763. http://dx.doi.org/10.1039/C0SM00579G.